Sipila, Seppo; Varje, Jari; Johnson, Thomas; Bilato, Roberto; Galdon-Quiroga, Joaquin; Snicker, Antti; Kurki-Suonio, Taina; Sanchis, Lucia; Silvagni, Davide; Gonzalez-Martin, Javier; ASDEX Upgrade Team; EUROfusion MST1 Team

ASCOT orbit-following simulations of ion cyclotron heating with synthetic fast ion loss diagnostic : a first application to ASDEX Upgrade

Published in:
Nuclear Fusion

DOI:
10.1088/1741-4326/ac0e71

Published: 01/08/2021

Document Version
Peer-reviewed accepted author manuscript, also known as Final accepted manuscript or Post-print

ASCOT orbit-following simulations of ion cyclotron heating with synthetic fast ion loss diagnostic: a first application to ASDEX Upgrade

Seppo Sipilä[1], Jari Varje[1], Thomas Johnson[2], Roberto Bilato[3], Joaquín Galdón-Quiroga[3], Antti Snicker[1], Taina Kurki-Suonio[1], Lucia Sanchís[1], Davide Silvagni[3], Javier González-Martín[5], the ASDEX Upgrade Team[6] and the EUROfusion MST1 Team[7]

[1] Department of Applied Physics, Aalto University, PO Box 14100, 00076 AALTO, Finland
[2] Fusion Plasma Physics, Department of Electric Energy Engineering, KTH, 10044 Stockholm, Sweden
[3] Max-Planck-Institute for Plasma Physics, Boltzmannstrasse 2, 85748 Garching, Germany
[4] Department of Atomic, Molecular and Nuclear Physics, University of Seville, 41012 Seville, Spain
[5] Department of Mechanical Engineering and Manufacturing, University of Seville, 41092 Seville, Spain
[6] See the author list of H. Meyer *et al.*, 2019 Nucl. Fusion **59** 112014
[7] See the author list of B. Labit *et al.* 2019 Nucl. Fusion **59** 086020

E-mail: seppo.sipila@aalto.fi

Accepted for publication in Nuclear Fusion 24 June 2021
https://doi.org/10.1088/1741-4326/ac0e71

Abstract

The orbit-following Monte Carlo code ASCOT interfaced with the radiofrequency Monte Carlo library RFOF can simulate radiofrequency heating of ion populations using wave solutions from full-wave solvers such as TORIC. It is applied to fundamental mode ion cyclotron resonant heating of hydrogen and 2nd harmonic frequency heating of neutral beam injected deuterium in ASDEX Upgrade discharge #33147 to validate the model against fast ion loss detector measurements. In addition, for FILD signal simulations requiring enhanced resolution or scanning the effect of various perturbations such as magnetohydrodynamic phenomena near the plasma edge, a two-stage simulation scheme is presented where the fast ion population is first created by a full ASCOT-RFOF ion cyclotron heating simulation, and the resulting distribution is then used as input to ASCOT's distribution-sampling marker source module for more efficient simulation of the ICRH ion wall load and FILD signal. A satisfactory agreement with experimentally observed FILD signal is found.

Keywords: orbit-following, Monte Carlo, ion cyclotron resonance heating, ASDEX Upgrade, wall loads, fast ion loss detector

1. Introduction

A good understanding of the fast ion confinement and transport properties of magnetic fusion devices is an important aspect in the progress towards reactor-scale experiments such as ITER and DEMO. The fusion-born alpha particles and the power load they deposit on the first wall are of primary interest, but the proposed radiofrequency heating and current drive schemes, with absorbed power in the range of tens of megawatts, are also potential sources of high local wall loads due to escaping RF-heated ions.

In combination with other diagnostics, fast ion loss detectors (FILD) [1] make it possible to gain knowledge of the transport of fast ions and the loss mechanisms that are involved. While not able to distinguish between ion

species, the FILD signal includes information of the fast ions' energy and pitch, offering insight into their origin and source of energy. Being able to simulate the FILD signal in realistic, machine-specific geometry and magnetic background can help interpret measured results and offers an efficient tool for, e.g., optimizing the position of the detectors or gaining better insight into the fast ion generation mechanisms and transport processes that are involved.

ASCOT [2] is a Monte Carlo orbit-following code for neoclassical charged particle studies in toroidal fusion devices. Developed in collaboration at Helsinki University of Technology (now Aalto University) and VTT since the early 1990's, it has evolved into a versatile tool that is widely used by the fusion research community to model fast ion populations in, e.g., ITER [3], JET [4], W7-X [5] and ASDEX Upgrade [6]. It is also implemented as part of the European Transport Simulator (ETS) in the context of the European Integrated Modelling project (EU-IM), the JINTRAC system of tokamak physics codes [7] and the ITER Integrated Modelling & Analysis Suite (IMAS) [8].

Until recently, ASCOT has featured fast ion sources for fusion products using the AFSI [9] module and realistic neutral beam injection using BBNBI [10]. It has been successfully benchmarked to, e.g., absolute measurements of fast ion losses in ASDEX Upgrade in the case of heat load to FILD arising from NBI deuterons [11] and against gamma-ray spectroscopy (GRS) and neutron emission spectroscopy (NES) diagnostics in a third harmonic ICRF scenario [12]. Simulation tools are, however, also needed for studying ion cyclotron resonance heating (ICRH) and its possible synergies with other fast ion sources, which is an active field of study in present-day plasma experiments [13,14] as well as in future reactor-scale devices such as ITER [15] and DEMO [16], where also the ICRH-related fast ion heat load distributions on the first wall are significant. For such simulations, we present ASCOT-RFOF, consisting of ASCOT interfaced with the radiofrequency heating code library RFOF [17,18], The work is structured as follows.

Section 2 describes the main features of ASCOT and RFOF as well as recent code developments that have made the present work possible.

In Section 3, ASCOT-RFOF is applied to fundamental mode ion cyclotron resonant heating (ICRH) of initially Maxwellian hydrogen and to second harmonic ICRH of NBI deuterium in the thoroughly diagnosed ASDEX Upgrade discharge #33147 at $t \cong 1$ s in order to demonstrate the evolution of a steady-state fast ion tail distribution.

In Section 4, the four-dimensional fast ion distributions generated in the heating simulations of Section 3 are used as a source distribution for sampling fast ion markers in dedicated fast ion wall load and FILD signal simulations. The results are compared to the experimentally observed FILD1 signal in ASDEX Upgrade discharge #33147.

Section 5 sums up the conclusions and discusses future work.

2. Model and methods

Version 4 of ASCOT can follow the guiding centers and gyro orbits of charged particle markers all the way to a fully three-dimensional first wall in 3D magnetic backgrounds of tokamaks and stellarators, taking into account both periodic asymmetries such as toroidal field ripple and MHD modes, and non-periodic perturbations such as, e.g., ITER's ferritic test blanket modules. The wall may be arbitrarily detailed and contain protruding elements such as FILDs, whose simulated signal can be derived from the overall ion wall load in postprocessing. The charged particle markers that are followed are weighted according to the number of real particles they represent in the source distribution of the studied population. Radial density and temperature profiles of the various plasma species, obtained from the experiment database, are used in this weighing as well as in Monte Carlo modelling of Coulomb collisions of the markers with an assumed Maxwellian background plasma, reproducing neoclassical transport in realistic geometry.

In simulating the wall load and FILD signal distributions, especially those from fast ions, following just the guiding center orbits of the ion markers will not yield realistic results. The orbiting ions typically approach the wall at a shallow angle, and omitting their finite Larmor radii causes them to hit the wall much further along their orbit than in the case of following the corresponding gyro orbit. In order to avoid this, ASCOT monitors the distance of the guiding center from the nearest triangular wall element and switches from guiding center formalism to full gyro orbit following when the marker's guiding center is within one gyroradius from the wall. This combines the computational efficiency of the guiding center formalism and the spatial accuracy of wall load simulation provided by the gyro orbit scheme, as long as the geometry of the device does not cause significant gyro orbit effects in particle transport, which may be the case in, e.g., spherical tokamaks.

ASCOT 4 has recently been interfaced with the RFOF ion cyclotron (IC) and lower hybrid (LH) interaction code library for orbit-following codes, making possible more realistic orbit-following Monte Carlo simulations of

radiofrequency heating and current drive than those demonstrated using simple phenomenological RF interaction models in early versions of [19].

RFOF, developed in the context of the European Integrated Modelling project, monitors the specified resonance condition along the ion markers' orbits. It predicts the time of resonance of the ion marker and adjusts the orbit-following time step accordingly, taking into account the Doppler shift of the resonance position due to the markers' parallel velocity. At resonance, RFOF evaluates a Monte Carlo operator for the wave-particle interaction to all orders in Larmor radius over perpendicular wave length, and modifies the marker's perpendicular velocity and energy to account for the energy transfer between the wave and the marker. It should be noted that the cyclotron resonance appears primarily in the gyrating perpendicular motion. The linear parallel motion does not experience a cyclotron resonance, except as a Larmor radius correction that can be neglected due the small parallel electric fields of the fast magnetosonic wave. Consequently, the parallel acceleration is neglected in RFOF.

All markers are followed for a time interval that is adequately long for achieving a statistically reliable rate of wave power absorption. Then, if needed, the wave electric field magnitude is adjusted to ensure that the absorbed power remains at the specified level. The time step between wave electric field adjustments needs to be long enough (of the order of milliseconds) to yield a statistically stable energy transfer rate, but not too long in order to avoid wasting computational resources in case the accumulated power transfer differs too much from the specified value. In ASCOT-RFOF's implementation, such failed time steps are cancelled and repeated with a readjusted wave electric field magnitude to ensure realistic power transfer at every time step.

As the latest improvement, ASCOT has been fitted with a distribution-sampling source module that uses as input a given four-dimensional distribution $f(R,z,\xi,E)$ where R and z are the major radius and vertical coordinate in [m], $\xi = v_{||}/v$ is the pitch and E is kinetic energy. The distribution is sampled to create markers for orbit-following simulations either beforehand or directly during the simulation. This makes it possible to study IC-heated ions in a computationally efficient two-stage scheme. In the case where the studied population is initially Maxwellian, a small auxiliary program is first run to create the four-dimensional Maxwellian plasma distribution $f_0(R,z,\xi,E)$ reflecting the plasma profiles of the species of interest in device-specific, realistic geometry. This source distribution is then used as input in an ICRH simulation, in which initially Maxwellian ion markers are sampled and simulated in ASCOT-RFOF in the presence of ICRH until a steady-state fast tail distribution $f_{IC}(R,z,\xi,E)$ is established. In the second stage, this obtained tail distribution is used in ASCOT as input for sampling ion markers in another simulation where all the markers represent only the fast ion population of interest, making it possible to, e.g., scan the effects of various edge-localized perturbations on the wall load distribution and FILD signal without the need to repeat the time-consuming heating phase. In the present scheme, the markers are sampled with equal weights using the acceptance-rejection method with linear 4D interpolation of the discrete distribution.

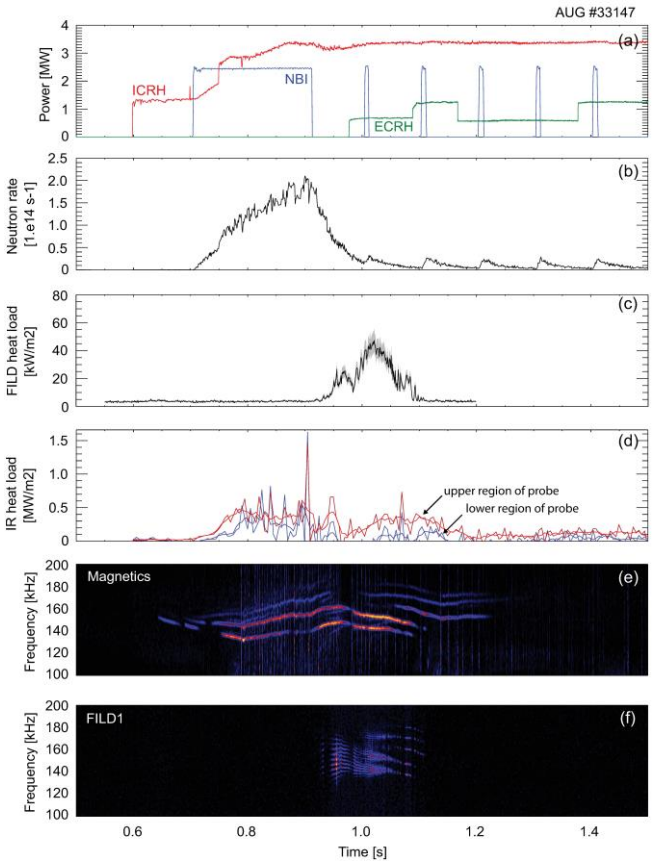

Figure 1. Main experimental signals for AUG discharge #33147 as a function of time. (a) heating power; (b) neutron rate; (c) fast ion heat load measured by FILD1; (d) total heat load at two different positions of FILD1 probe head in the R region of the pinhole, measured by the infrared diagnostic; (e) spectrogram of magnetic fluctuations; (f) spectrogram of FILD1 signal.

3. Ion cyclotron heating simulation

The thoroughly diagnosed ASDEX Upgrade discharge #33147 at $t \cong 1$ s was selected for modelling. The main experimental signals of this discharge, with a toroidal magnetic field of -2.487 T and a plasma current of 0.7 MA, are presented as a function of time in Figure 1. The density and temperature of the background plasma species, exported from AUG database as Integrated Data Analysis (IDA) [20] constructed

profiles, are shown in Figure 2. The hydrogen density and temperature in the IC heating simulation represent an isotropic Maxwellian hydrogen population equal to 5% of electron density at bulk ion temperature.

For the fundamental IC frequency heating simulation of hydrogen, an ensemble of 500.000 hydrogen markers was created with energies representative of the local Maxwellian bulk ion distribution and with random pitch ξ and random (R,ϕ,z) location. The markers were followed for 100 milliseconds, long enough to produce a statistically reliable steady state fast ion distribution with kinetic energies reaching about 2 MeV. The steady state was confirmed by monitoring the time evolution of the fast ion tail. Markers lost in wall collisions were replaced by new markers sampled from the bulk plasma distribution. This was done to prevent a diminishing number of markers absorbing the available IC wave power, which could have distorted the fast ion tail distribution towards ever higher energies.

The IC wave electric field components E^+ and E^-, evaluated for the same ASDEX Upgrade discharge and time, were obtained on an (R,z) grid from the full-wave hot-plasma toroidal simulation code TORIC-SSFPQL [21,22], and are shown in poloidal plane in Figure 3 with the fundamental ion cyclotron resonance layer of hydrogen marked with white dashed line. TORIC is a full-wave axisymmetric code for solving the propagation and absorption of ICRF waves, and is interfaced with the 2D kinetic solver SSFPQL for the distribution function of the ICRF and NBI ion species. TORIC provides the power deposition profiles to SSFPQL for the evaluation of the quasilinear operator, and SSFPQL in turn calculates the distribution functions of the heated species used to evaluate the plasma response in TORIC. Convergence is reached when the power deposition profiles calculated by the two codes differ less than a tolerance value set by the user. In this case the tolerance was set to 1%. Because of the competition between first-harmonic absorption by H with the second-harmonic absorption by D, about 8 iterations between TORIC and SSFPQL were necessary to reach convergence. Figure 3(b) also depicts a simulated IC-heated 1 MeV hydrogen ion orbit with the banana tips at the resonance layer. The negative pitch leg is shown in blue and the positive pitch leg in red.

In order to reduce the computation time consumed by RFOF in keeping track of the markers' resonance condition and in calculating

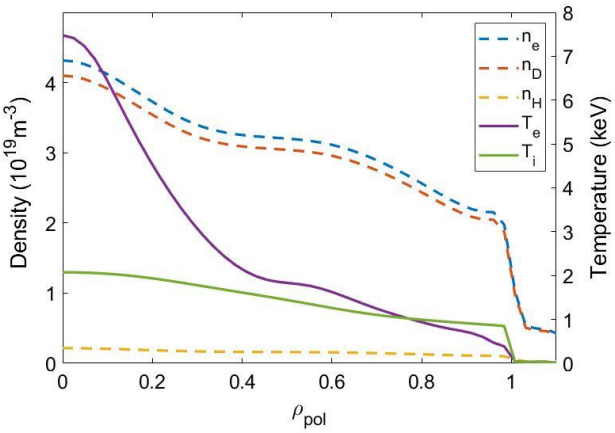

Figure 2. Plasma profiles as a function of ρ_{pol} for ASDEX Upgrade discharge #33147 at t = 1.003 s. The shown deuterium and electron density and temperature are imported into ASCOT from AUG database (IDA). The lowest curve shows the assumed hydrogen population (5% of electron density), with a corresponding reduction assumed in deuterium density in order to maintain charge quasineutrality.

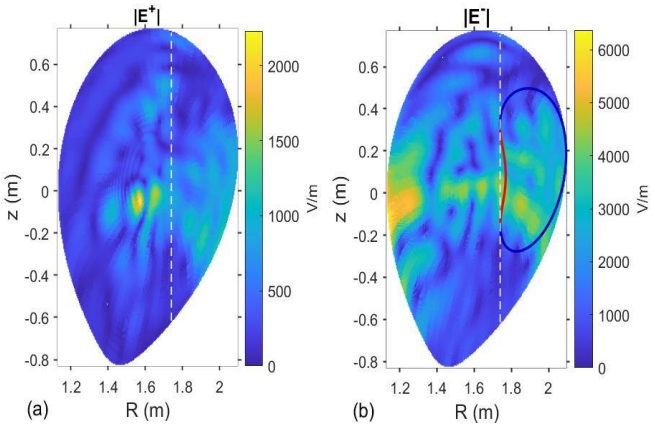

Figure 3. The left-hand (a) and right-hand (b) circularly polarized components E^+ and E^- of the IC wave electric field (superposition of n_ϕ = ±13 modes) in ASDEX Upgrade discharge #33147 at t = 1 s, imported to ASCOT-RFOF from TORIC. The fundamental ion cyclotron resonance layer of hydrogen is shown in white dashed line. To demonstrate the wide orbits of strongly heated ions, a 1 MeV hydrogen ion guiding-center orbit is depicted in (b). The negative pitch leg is shown in blue (dark grey) and the positive pitch leg in red (light grey).

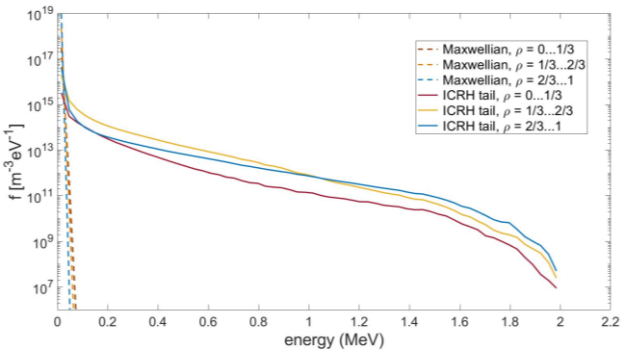

Figure 4. The steady-state tail distributions for a 5% hydrogen population heated by ICRH in a 100 ms simulation (solid lines) and the corresponding initial Maxwellian distributions (dashed lines) shown for three radial regions in the plasma.

energy transfer at resonance, only one antenna with frequency 36.5 MHz and two toroidal modes (n_ϕ = –13 and +13) was modelled by TORIC-SSFPQL. The selected frequency matches that used in ASDEX Upgrade discharge #33147, placing the resonance layer for fundamental mode IC heating of hydrogen at $R \cong 1.74$ m (excluding the Doppler shift), while the magnetic axis in this discharge was at $R \cong 1.66$ m. The power absorbed by the hydrogen population, as modelled by TORIC, was 2.29 MW (about 92% of the total absorbed IC power in discharge #33147 at $t = 1$ s).

In the ASCOT-RFOF heating simulation, a 5 ms simulation time step was used for wave electric field adjustment, as described in Section 2 in the context of RFOF. To ensure stable power absorption at the prescribed level, the time step was cancelled if the power absorption deviated too much (15%) from the given value. After such failed steps, all markers were returned to their previous state and their recorded contributions to the tail distribution during the failed step were cancelled. The wave electric field was then readjusted making use of the power absorption information gathered during the failed step. Such repetitions of a time step were occasionally observed in the beginning of the heating simulation, where the very first step was iterated two to four times, depending on how far off the mark the initial value given to the normalization factor was, until the prescribed power transfer was achieved.

At time $t \cong 1.0$ s in discharge #33147, only one neutral beam (NBI3) was active. NBI3 injected deuterons at 2.57 MW power and 60/30/20 keV energies during a 200 ms pulse after $t \cong 0.7$ s, as shown in Fig. 1(a). The presence of fast deuterons from neutral beam injection was omitted in the IC heating simulation of hydrogen markers. The justification for this is that the fast NBI-injected deuterium population (possibly experiencing second-harmonic IC heating) would be very small compared to the bulk deuterium population, and can thus be assumed insignificant in the simulated hydrogen markers' collisional interactions with bulk deuterium, assumed by ASCOT's Monte Carlo collision model to have a Maxwellian energy distribution.

The hydrogen tail distribution generated by ASCOT-RFOF in a 100-millisecond simulation of fundamental mode ion cyclotron resonance

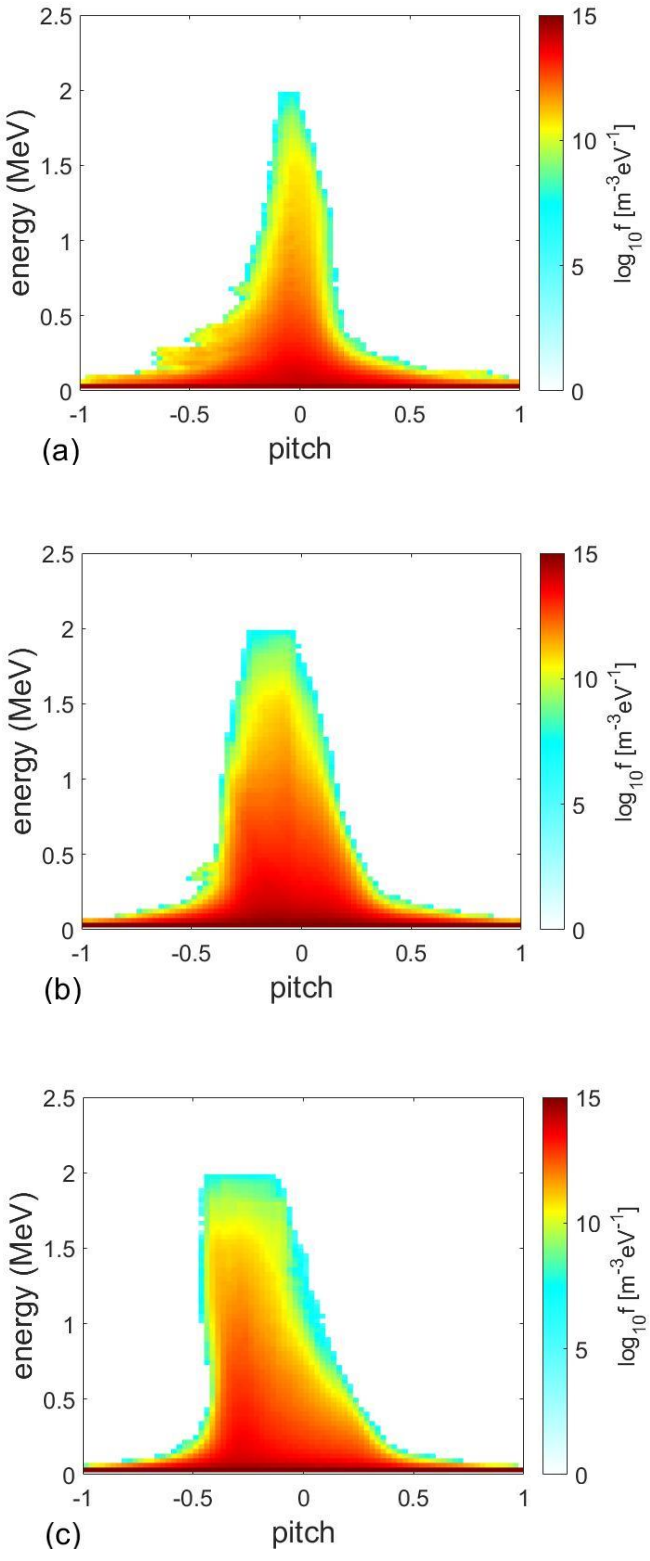

Figure 5. Energetic hydrogen tail distribution $f_{IC}(R,z,\xi,E)$ in pitch-energy space, sampled from the IC-heated distribution of a 100 ms ASCOT-RFOF heating simulation, in three radial regions: (a) ρ_{pol} = 0…1/3; (b) ρ_{pol} = 1/3…2/3; (c) ρ_{pol} = 2/3…1.

heating is shown in Figure 4 as a function of energy for three radial regions. The tails of the markers' initial local Maxwellian distribution are also shown.

The significance of a proper 4D source distribution in toroidal-geometry fast ion simulations is demonstrated in Figure 5, showing the simulated ICRH tail distributions as a function of pitch ($\xi = v_{\|}/v$) and energy. In Figure 5(a), the IC-heated tail distribution in the region closest to the magnetic axis (poloidal flux surface coordinate ρ_{pol} = 0…1/3) is found to be slightly asymmetric in pitch, with a bigger population on the negative-pitch side especially at energies below 1 MeV. This is a consequence of the orbit topologies of the heated ions, shown in Figure 6 (for a detailed analysis of orbit dynamics in tokamaks, see [23]). The trapping cone is narrow in this region, and the passing particles with negative pitch are at the outermost poloidal flux surfaces of their orbits on the outboard side where the IC resonance is located (about 8 cm outwards from the magnetic axis along the equator, on poloidal magnetic flux surface $\rho_{pol} \cong 0.244$ at the equator).

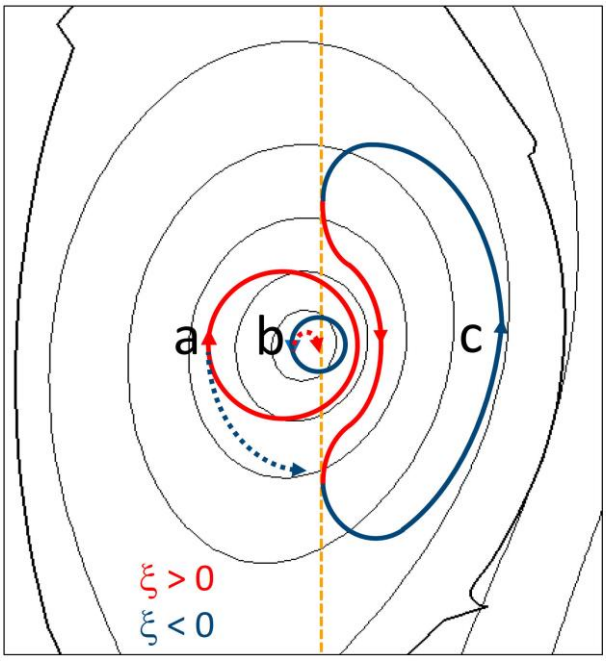

Figure 6. Schematic showing AUG orbit topologies of ions interacting with the IC wave at the resonance layer (shown in orange). Positive pitch ξ is shown in red (light grey) and negative pitch in blue (dark grey). The deviation from magnetic surface is exaggerated to clarify the differences. Dotted lines show how the orbit topology eventually changes from passing to trapped as perpendicular energy is absorbed from the wave. a) co-passing orbit; b) counter-passing orbit; c) fully developed IC-heated trapped (banana) orbit with tips at the resonance layer. Counter-passing and trapped orbits (b and c) are at their outermost flux surface at the outermost equator crossing in major radius; in the case of co-passing orbits (a), the outermost flux surface of the orbit is at the inboard side equator crossing.

Thus, negative-pitch passing ions contribute more to the IC-heated tail distribution at the innermost magnetic surfaces, until their orbits eventually turn into trapped (banana) orbits due to the perpendicular energy absorbed from the IC wave. After that, they contribute to the IC-heated tail distribution both at negative pitch (on the longer outer leg of their orbits) and positive pitch (on the shorter inner leg of their orbits).

Positive-pitch passing ions in this ρ_{pol} region, on the other hand, are on the innermost magnetic surfaces of their orbits in the IC resonance layer. They contribute to the positive-pitch side of the IC-heated tail distribution (and towards outer magnetic surfaces) until the perpendicular energy transfer from the IC wave flips them onto trapped orbits. After that, they too will contribute to the negative-pitch side of the distribution on the longer outer leg of their trapped orbits, and to the positive-pitch side on the shorter inner leg of their orbits. The asymmetry in pitch is also seen in the region ρ_{pol} = 1/3…2/3, as shown in Figure 5(b). In the outermost region (ρ_{pol} = 2/3…1), the IC-heated tail is visibly skewed towards negative pitch, as shown in Figure 5(c). This is to be expected, as the trapping cone is wide in the outermost region and the IC-heated ions tend to end up on trapped orbits with their tips at the resonance layer. IC-heated ions that contribute to this outermost layer are predominantly on the negative-pitch outer leg of their trapped orbits. In order to check the effect of the prescribed absorbed IC power, it was adjusted to just 2 MW instead of 2.5 MW. The resulting energetic tail of the hydrogen distribution was found to be correspondingly lower in terms of density, but reached the same maximum energy of about 2 MeV.

Neutral beam injection was also present in discharge #33147 shortly before t ≅ 1.0 s (at about 0.7-0.9 s at 2.57 MW power from NBI source 3). To check for a synergy effect of NBI and ICRH, a simulation of second harmonic IC heating of NBI deuterium was made assuming NBI3 to be on, using the equilibrium at t = 1 s and assuming an E^+/E^- ratio of about 0.1, with 8% of the total absorbed IC power going to the NBI deuterons. NBI-ICRH synergy was demonstrated by the formation of a tail distribution reaching about 600 keV energy over 100 ms, as shown in Figure 7.

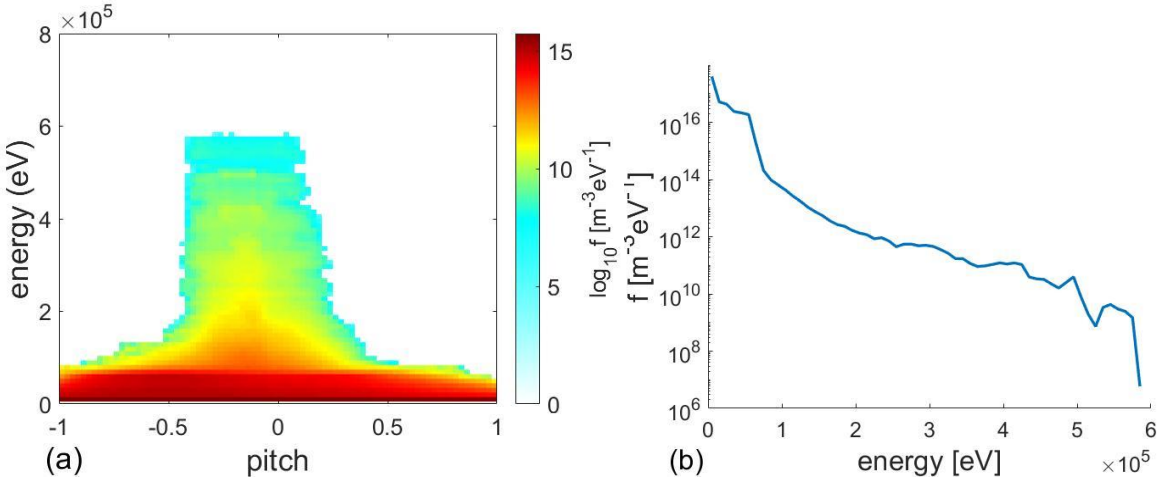

Figure 7. (a) The IC-heated NBI deuterium tail distribution as a function of (a) pitch and energy, and (b) energy. The data is collected over the whole poloidal cross-section (ρ_{pol} = 0…1). The highest initial NBI energy of 60 keV is seen as a sharp transition from red to orange in (a) and as a dip in the tail distribution in (b).

Examples of the wall load distributions from the IC heating simulations are shown in Figure 8 for (a) 5% H (a) and (b) NBI D. FILD2, one of the two FILDs present in ASDEX Upgrade discharge #33147, is also visible protruding from the outboard wall. In the hydrogen simulation, 922 marker hits on FILD1 probe head were recorded in this simulation. While escaping low-energy hydrogen markers end up in the divertor, as per design, escaping fast ion markers hit the FILD and other protruding elements such as ICRF antenna edges higher up on the outboard wall. With the present simulation parameters and assumptions, the hot spots on the wall experience a heat load of the order of 5 MW/m^2.

The peak wall loads arising from the NBI D IC heating simulation were found at the ICRH antenna edges and the FILD, as in the case of hydrogen, and were of the order of 1 MW/m^2, as shown in Figure 8(b). The wall load distribution is qualitatively consistent with images taken from the video real time (VRT) diagnostic, where the edges of the ICRF antennas are observed to glow during the time interval of interest, indicating increased temperature of these components due to an increased power load.

4. Simulation of FILD signal sampling only fast ion markers

Simulating the FILD signal with ASCOT is based on 3D models of the detectors protruding from the first wall. It is assumed that the velocity components of a fast ion do not change much within the small volume occupied by the FILD, and the actual pinhole of the detector is not modelled (obtaining reasonable signal statistics through the pinhole would require an excessive amount of computing time, as the FILD, let alone its pinhole, is a very small target for the limited number of fast ion markers that can be modelled with available computing resources). The signal is obtained in the same manner as for the rest of the wall load, i.e. by recording marker hits with their weight factor and energy for each individual triangular element of the wall and FILD. The markers hitting the wall triangles that belong to a specific FILD are postprocessed into a hit map as a function of their gyroradius and pitch angle,

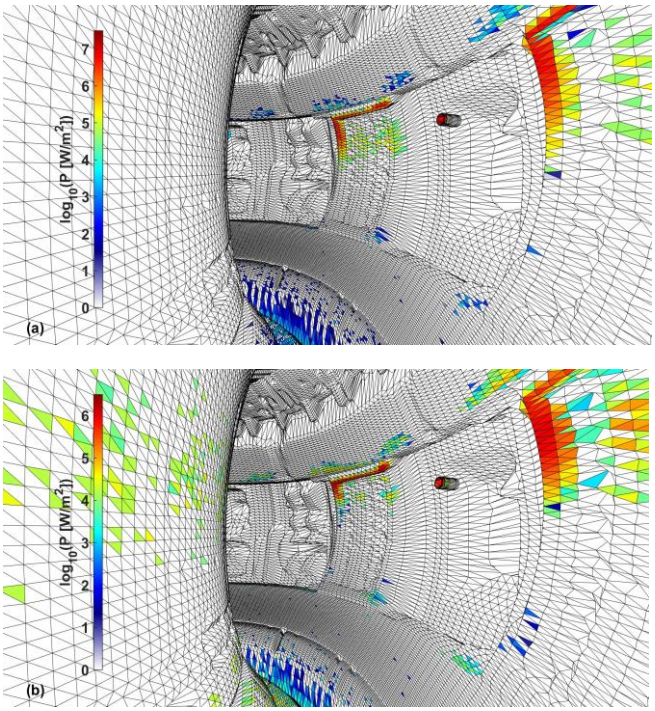

Figure 8. The wall load distribution recorded from the ICRH heating simulation with just toroidal field ripple present for (a) an assumed 5% H population, (b) NBI D. One of the two FILDs active in ASDEX Upgrade discharge #33147 (FILD2) can be seen protruding from the outer wall.

defined as 180°–acos($v_{||}/v$). This yields an unrefined simulated FILD signal, as the instrument response is not yet taken into account.

The hit maps from the ICRH simulations with only toroidal field ripple perturbing axisymmetry, as recorded directly from ASCOT-RFOF simulation, are shown for hydrogen and NBI deuterium in Figure 9. While the IC-heated hydrogen presents a strong concentration of hits at energies of several hundred keV, only sporadic hits of NBI deuterium are seen in FILD1, and their gyroradii indicate energies below 50 keV. On FILD2, which is at the same poloidal location as FILD1 but in the neighboring quadrant of NBI source #3, a clear signal is recorded for each of the initial NBI beam energies (60, 30 and 20 keV), as shown in Fig. 9(c). It is obvious that especially in the case of NBI D, the statistics of the IC heating simulation are not adequate to yield a proper signal from the IC-heated tail distribution.

While a simulation starting from a Maxwellian marker population and applying IC heating models the evolution of the tail distribution in a physics-wise more complete manner and gives a more complete picture of wall load distributions, it is inefficient in simulating the FILD signal. The hit map shown for hydrogen in Fig. 9(a) indicates ion energies in excess of 100 keV. In this energy range, the computational efficiency of simulating fast ion wall loads and FILD signal from a Monte Carlo orbit-following simulation starting from a Maxwellian population will be poor, as a great majority of markers will spend most of their time below the high energy range of interest observed by FILD1 in experiment.

Especially in simulations scanning the effects caused by various perturbations on the wall load distribution and/or FILD signal, e.g., resonant magnetic perturbation (RMP) coils or ITER's ferritic inserts at toroidal field coils, it is computationally more efficient to sample markers only from the tail distribution. This is facilitated by ASCOT's distribution-sampling marker source module.

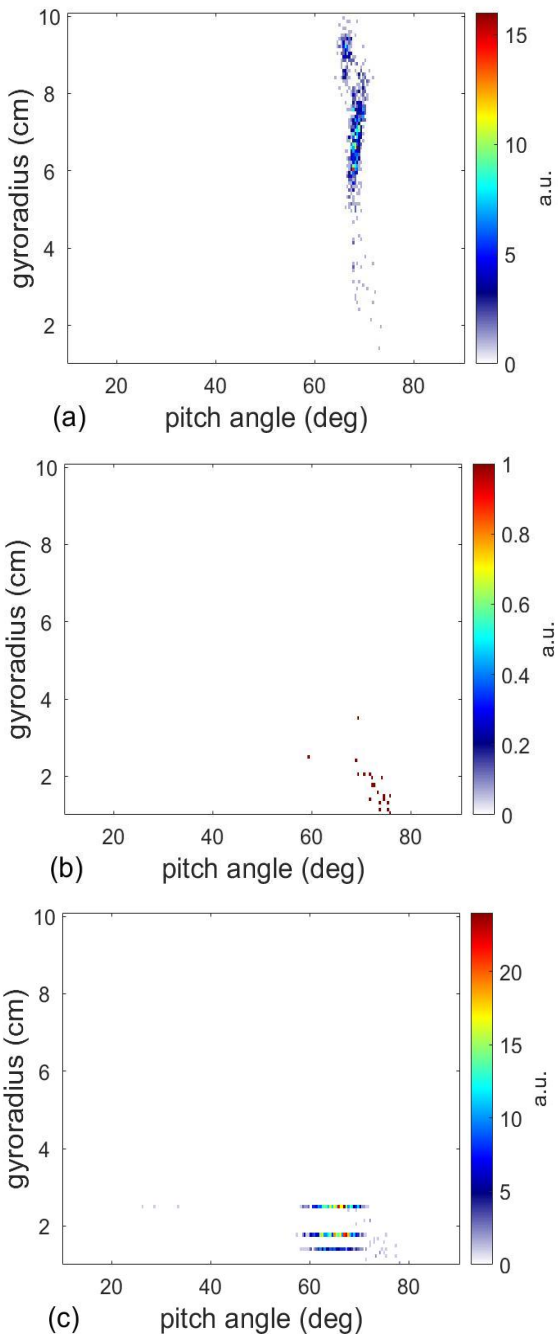

Figure 9. FILD1 marker hit distribution from ASCOT-RFOF ICRH simulation. (a) FILD1, 5% hydrogen population; (b) FILD1, NBI source #3 deuterium; (c) FILD2, NBI source #3 deuterium. The colormap scales are in arbitrary units but comparable to each other.

To demonstrate this, FILD signal simulations were made sampling fast hydrogen markers from the IC-heated 4D distribution $f_{IC}(R,z,\xi,E)$ obtained in the ICRH simulation described in the previous section. As the time scale of fast ion losses can be assumed short compared to that of significant IC heating, ICRH was not present in the FILD signal simulation. The distribution-sampling source module of ASCOT was limited to producing markers of at least 85 keV energy, near the low end of the FILD's gyroradius range for hydrogen in the present magnetic field.

Markers were sampled and simulated until a prescribed number of marker hits on FILD1 was achieved. As the source distribution obtained from the IC heating simulation already contains the effects of transport by collisions and toroidal field ripple (as well as other modelled perturbations such as MHD and/or anomalous diffusion), the FILD simulation markers were followed for just 0.1 ms (~100 orbits) to allow those on the verge of escaping to

get out. Coulomb collisions of the markers with the Maxwellian bulk plasma were also switched off, as their effect on the orbits is very small on such short time scale. Using this approach, the computational efficiency of producing fast ion hits on the FILD was enhanced by a factor of 58 (see Appendix for details).

Examples of the IC-heated ion wall loads recorded in the FILD signal simulations are shown in Figure 10. The load distributions on FILD1 probe head from the fast ion simulations are shown in Figure 11. In addition to the improved statistics of the fast ion load distribution on the upper wall, as demonstrated by comparing the load distributions on the ICRH antenna surface to those obtained from the IC heating simulation (Figure 8), the obvious difference to the heating simulation result is the absence of all low-energy marker hits in the divertor region.

The unrefined FILD1 signal from the fast ion simulation is shown in Figure 12 for hydrogen in the ripple-only case (a) and including MHD (b). In the present study, the MHD phenomena modelled consisted of a (2,1) neoclassical tearing mode (NTM) island at about mid-radius in ρ_{pol} [24] and toroidal Alfvén eigenmodes (TAE, based on the LIGKA model [25]) relevant to the selected discharge. For the NTM, electron cyclotron emission (ECE) measurements were used to detect the island width, which was then tuned in the simulations to match the experimental value. For the TAEs, Mirnov coil measurements were used to estimate the perturbation of the magnetic field, which was then modified accordingly in the simulations. The corresponding signals with and without MHD obtained for IC-heated NBI deuterium are shown in (c) and (d), respectively. For deuterium, the IC-heated source distribution is sampled only at energies above 75 keV to filter out the initial NBI energies and their collisional tail above 60 keV.

To demonstrate the simulated FILD signal sensitivity to the details of the simulation setup, Figure 12(e) and (f) show, respectively for H and NBI D, the result obtained by sampling energetic markers from the IC-heated tail distribution obtained in an unperturbed, axisymmetric IC heating simulation. In this case, without any perturbations to the magnetic background, the radial transport of ion markers is much weaker (purely neoclassical), leading to a more localized signal distribution at higher gyroradius.

In order to compare the simulated FILD1 signal to the experimentally measured signal in AUG discharge #33147, the instrument response of the detector needs to be taken into account.

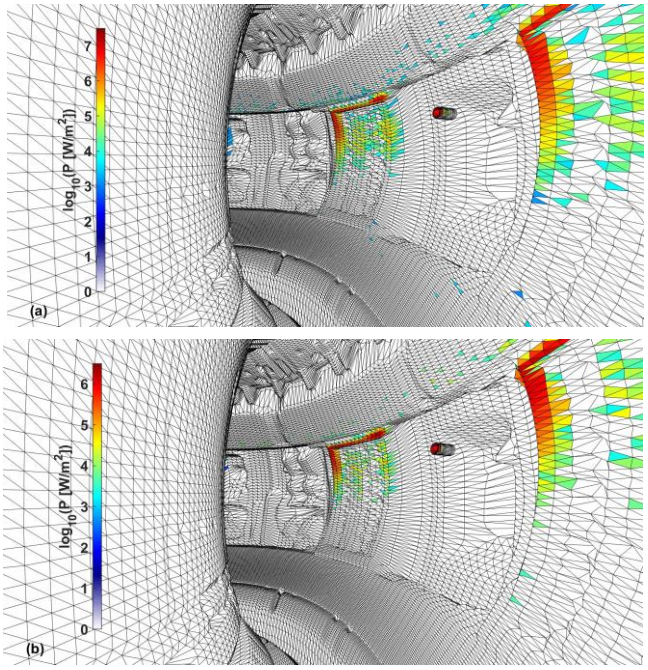

Figure 10. The wall load distribution recorded from the fast ion simulation, with just toroidal field ripple present (a) sampling H markers above 85 keV energy with only toroidal field ripple present; (b) sampling IC-heated NBI D markers above 75 keV. Compared to the ICRH heating simulation results shown in Fig. 8, the computational efficiency of simulating fast ion wall loads is greatly enhanced by simulating only ion markers sampled from the tail distribution.

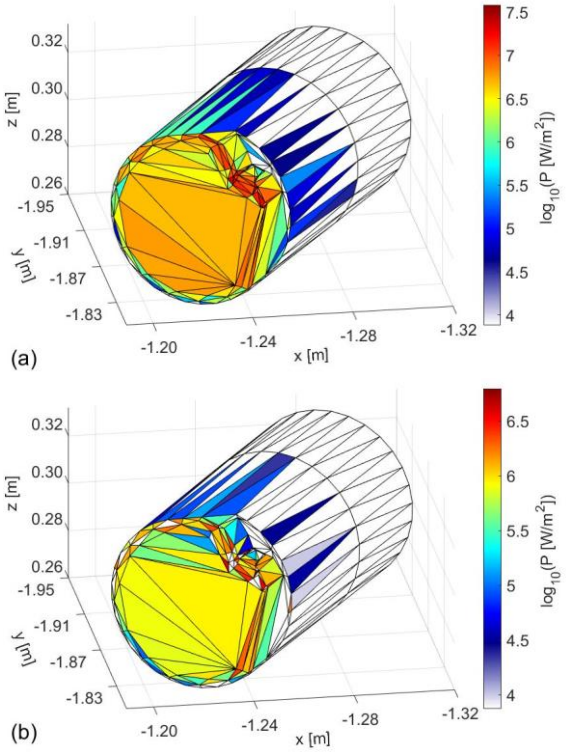

Figure 11. FILD1 geometry with superimposed ICRH-heated ion heat load with ripple only present from (a) the assumed 5% H population; (b) from NBI D.

This is done in the final postprocessing phase by the FILDSIM code [26] that modifies the recorded hit distribution on the FILD to represent the distribution on the scintillator plate. FILDSIM takes into account the realistic 3D geometry of the detector and the photon yield of the scintillator to generate a synthetic signal that can be directly compared to the experimental measurement.

The time-integrated measured FILD1 signal is shown in Figure 13(a), and the instantaneous measured signal at two instants of time close to t = 1 s are shown in Figure 13(b) and (c). For comparison, the simulated and FILDSIM-postprocessed signal from the IC-heated tail distribution of the assumed 5% hydrogen population is shown for toroidal field ripple only (d) and with MHD included (e), while (f) and (g), respectively, show the same for 2nd harmonic heating of NBI deuterium. The simulated signal in Fig. 13(d) and (e) can be seen to extend to gyroradii larger than those observed in experiment, suggesting that with the assumptions made, the simulation is slightly overestimating the energies of the H ions reaching the FILD detector. A possible explanation for this is the omission of gyromotion in the heating simulation (except near the wall) and the related radial transport mechanisms [27] that are thus not present. Especially in the case of hydrogen, with gyroradii in AUG of about 7 cm at 1 MeV kinetic energy, the simulation may overestimate the confinement time of the ion markers, allowing them to interact with the wave for a longer time than in experiment. Gyromotion, however, is not implemented in the current ICRH model, and the computational cost of a full orbit heating simulation would be prohibitively high.

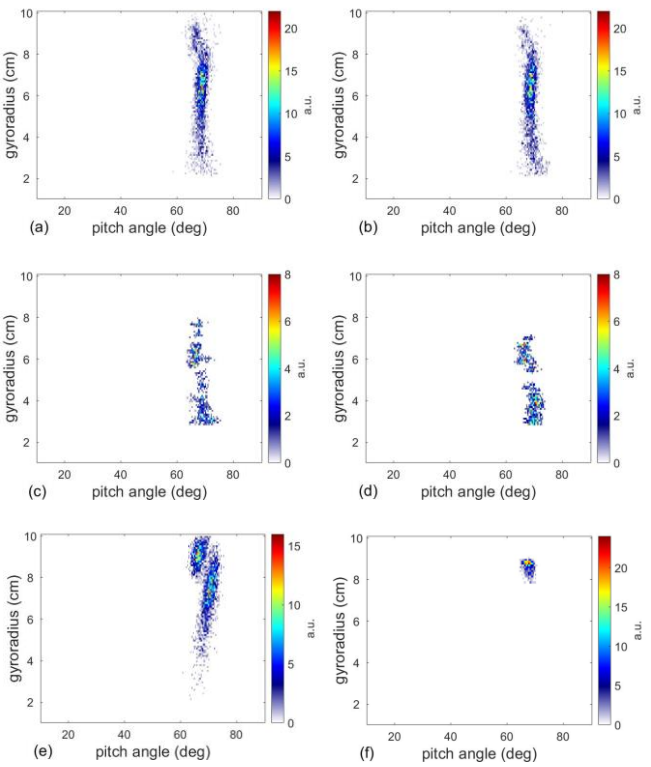

Figure 12. The marker hit distribution in pitch angle and gyroradius on FILD1 from ASCOT-RFOF simulation of (a) IC-heated hydrogen tail distribution sampled only at energies above 85 keV with only toroidal field ripple present; (b) same with MHD included. 3000 FILD1 hits were recorded in both simulations. The marker hit distribution on FILD1 for IC-heated NBI D above 75 keV is shown in (c) for only toroidal field ripple present and in (d) for MHD also included. In these two cases, 750–1000 FILD1 hits were recorded. (e) and (f) show, respectively for H and NBI D, the result of sampling fast ion markers from the IC-heated tail distribution obtained in an unperturbed axisymmetric IC heating simulation.

A slight pitch angle discrepancy between measured and simulated signal is also observed. The FILD strike map was calculated with and without considering the toroidal field ripple, and a negligible impact on the measured pitch angle distribution was found. A small misalignment of the strike map is a possible explanation for the discrepancy, but other physics reasons cannot be fully excluded.

A reasonable agreement with experiment is found, though, taking into account the simplified setting of the simulation with a fixed equilibrium and the absence of time-dependent phenomena that cause the measured FILD1 signal to fluctuate with time, as can be seen from the two instantaneous signals shown in Fig. 13(b) and (c). A possible explanation for the observed fluctuation is a beat effect between the NTM and TAEs.

Comparing the simulated heat loads on the probe head (Fig. 11) to results from IR imaging, shown in Fig. 1(d), the simulated hydrogen loads are found to be too high by a factor of 5–10. This suggests that the ICRH tail distribution is overestimated. One underlying reason for this is likely to be the assumption of the 5% hydrogen population absorbing all of the 2.5 MW ICRH power that is not going to NBI D. In a sensitivity scan of IC power assuming just 2.2 MW of ICRH power leaving the antennae (the lower limit of its fluctuation) to be absorbed by H and NBI D, and then only 1.9 MW to allow, e.g., for parasitic absorption, the simulated heat load on the FILD1 probe head was found to diminish by a factor of 2…3.

Another factor affecting the hydrogen heat load is the assumed size of the H population. A sensitivity scan of the ICRH heating simulation to the H population size, assuming the IC wave solution to remain valid, revealed that the number of fast hydrogen markers hitting FILD1 goes strongly down with increasing H population. This stands to reason as the available heating power per hydrogen ion diminishes with increasing hydrogen population.

On the other hand, with a larger H population each of the 500.000 markers represents correspondingly more real ions, compensating the effect of fewer FILD hits to some extent. The overall effect of increasing the H population size in the range 3%...7% was a factor of 2 reduction in the simulated FILD1 heat load.

In the case of 2nd harmonic heating of NBI deuterium, where the NBI source density is known and about 8% of the ICRH power is assumed to go to NBI D, the heat loads on the probe in the pinhole region were found to be of the same order of magnitude with the IR imaging result. It should be kept in mind, however, that at the time of measurement NBI had not been active for about 100 ms. On the other hand, before the NBI was turned off, it had been on for about 200 ms simultaneously with ICRH, allowing a D tail distribution to form and persist, as ICRH was active throughout the time interval of interest. The presence of such a residual ICRH-heated NBI tail at the time of measurement is thus possible.

While the experimentally observed FILD1 signal distribution was reasonably reproduced in simulation, modelling the heat loads with better quantitative accuracy would require detailed knowledge about the actually absorbed ICRH power and the way it is divided between various absorbers.

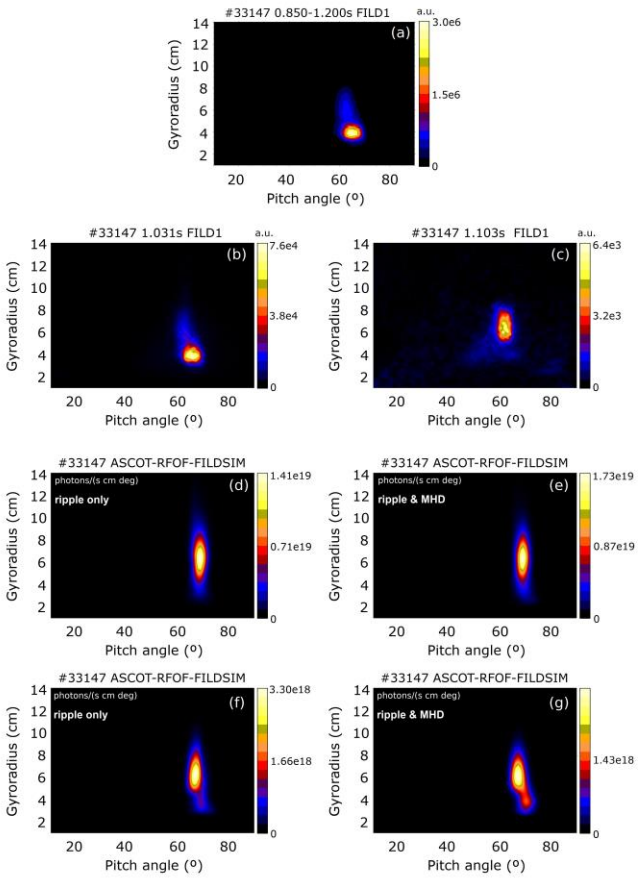

Figure 13. (a) measured FILD1 signal integrated over the time window of interest; (b) and (c): measured instantaneous FILD1 signal at t = 1.031 s and t = 1.103 s, respectively; (d) and (e): the signal from IC-heated 5% H population simulated by ASCOT-RFOF-FILDSIM with toroidal field ripple only and with MHD included, respectively; (f) and (g): the signal from IC-heated NBI deuterium (source #3) simulated by ASCOT-RFOF-FILDSIM with toroidal field ripple only and with MHD included, respectively.

5. Conclusions and future work

The capability of ASCOT-RFOF to simulate the forming of a steady-state IC-heated tail distribution has been demonstrated using the magnetic background, plasma and wall data for the thoroughly diagnosed ASDEX Upgrade discharge #33147 at t = 1 s. A steady-state tail distribution was shown to develop in fundamental frequency heating of an assumed 5% population of bulk hydrogen and in second harmonic frequency heating of NBI deuterium.

The 4D energetic tail from the heating simulation was then used as a fast ion marker-sampling source distribution for simulating the fast ion wall load and FILD1 signal, achieving greatly improved statistics. With postprocessing of the simulated hit distribution on FILD1 with FILDSIM in order to take into account the instrument response, a reasonable agreement with the measured FILD1 signal was found in terms of the velocity space distribution of the fast ion losses.

The described simulation scheme opens up possibilities for simulating IC-heated wall loads and diagnostics signals in realistic case-specific 3D geometry and wall configuration. For example, as ITER is going to have a total of 20 MW of ion cyclotron heating power, modelling the wall loads arising from IC-heated ions in realistic ITER geometry is an obvious application of ASCOT-RFOF in the near future. To facilitate this, ASCOT-RFOF has also been implemented in the Integrated Modelling and Analysis Suite (IMAS) environment. Augmenting ASCOT-RFOF with dynamic ion marker sources for beam-target, beam-beam and thermonuclear fusion products from AFSI is also under development. This will facilitate studies of possible harmonic-frequency ICRH power absorption and wall load distribution of fusion products arising from, e.g., IC-heated NBI ions.

Acknowledgements

The ASCOT-RFOF simulations were carried out using the Marconi-Fusion supercomputer at CINECA, Bologna, Italy. This work has been carried out within the framework of the EUROfusion Consortium and has

received funding from the Euratom research and training programme 2014–2018 and 2019–2020 under grant agreement No 633053. The views and opinions expressed herein do not necessarily reflect those of the European Commission. This work was partially funded by the Academy of Finland project 298126.

Appendix: Computational requirements and efficiency

A 100 ms IC heating simulation of a 5% hydrogen population in 3D magnetic background with toroidal field ripple present, using 500.000 markers and replacing lost markers with new thermal ones, took about 18 hours using 3072 cores on EUROfusion Marconi's A3 (Skylake) partition. In the presence of MHD, the number of simulated markers had to be lowered from 500.000 to 200.000 due to the computational requirements of the MHD model. Each marker thus represented 2.5 times as many real ions as in the corresponding ripple-only case.

A FILD signal simulation producing 3000 hydrogen marker hits on FILD1 took just 1 hour using 3072 cores on EUROfusion Marconi's A3 partition. Achieving this number of FILD1 hits required the sampling and following of about 38 million fast ion markers, but as the time limit of this simulation was just 1/1000 of what was used in the corresponding IC heating simulation, the overall CPU efficiency (FILD hits per CPU second) of simulating the FILD signal in this was found to be 58-fold for the 5% hydrogen case.

In the second-harmonic deuterium case, sampling fast ion markers took much more CPU time due to the weaker ICRH tail. As a result, fewer FILD1 hits accumulated in this simulation per unit CPU time even when sampling markers was additionally restricted to $\rho_{pol} > 0.5$. Only 750–1000 FILD1 hits were obtained in 24 hours of computing time. Nevertheless, simulating the FILD signal from IC-heated NBI D this way was found to be feasible, which was not the case in the IC heating simulation, as demonstrated in Fig. 9(b). The CPU efficiency (FILD hits per CPU second) was found to be 21-fold in this case as compared to the NBI D heating simulation.

References

[1] García-Muñoz M *et al* 2009 *Rev. Sci. Instrum.* **80** 053503
[2] Hirvijoki E *et al* 2014 *Comput. Phys. Commun.* **185** 1310
[3] Kurki-Suonio T *et al* 2016 *Nucl. Fusion* **56** 112024
[4] Sirén P *et al* 2017 *J. Instrum.* **12** C09010
[5] Äkäslompolo S *et al* 2018 *Nucl. Fusion* **58** 082010
[6] Asunta O *et al* 2012 *Nucl. Fusion* **52** 094014
[7] Romanelli M *et al* 2014 *Plasma and Fusion Research* **9** 3403023
[8] Imbeaux F *et al* 2015 *Nucl. Fusion* **55** 123006
[9] Sirén P *et al* 2018 *Nucl. Fusion* **58** 016023
[10] Asunta O *et al* 2015 *Comput. Phys. Commun.* **188** 33
[11] Rodriguez-Ramos M *et al* 2017 *Plasma Phys. Control. Fusion* **59** 105009
[12] Salewski M *et al* 2017 *Nucl. Fusion* **57** 056001
[13] Joly J *et al* 2019 *Plasma Phys. Control. Fusion* **61** 075017
[14] Faustin JM *et al* 2016 *Plasma Phys. Control. Fusion* **58** 074004
[15] Schneider M *et al*, "Modelling one-third field operation in the ITER Pre-Fusion Power Operation phase". Preprint: 2018 IAEA Fusion Energy Conference, Gandhinagar IAEA-TH/6-1
[16] Van Eester D *et al* 2019 *Nucl. Fusion* **59** 106051
[17] Johnson T *et al* 2006 *Nucl. Fusion* **46** S433
[18] Johnson T *et al* 2011 AIP Conf. Proc. **1406** 373
[19] Heikkinen J *et al* 1997 *Nucl. Fusion* **37** 835
[20] Fischer R *et al* 2010 *Fusion Sci. Technol.* **58** 675
[21] Bilato R *et al* 2011 *Nucl. Fusion* **51** 103034
[22] Weiland M *et al* 2017 *Nucl. Fusion* **57** 116058
[23] Eriksson L-G and Porcelli F 2001 *Plasma Phys. Control. Fusion* **43** R145
[24] Kurki-Suonio T *et al* 2011 *Nucl. Fusion* **51** 083041
[25] Lauber Ph *et al* 2007 *J. Comput. Phys.* **226** 447
[26] Galdón-Quiroga J *et al* 2018 *Plasma Phys. Control. Fusion* **60** 105005
[27] Mimata *et al* 2008 *Progress in Nuclear Energy* **50** 638